
Evaluating Adversarial Robustness for Deep Neural Network Interpretability using fMRI Decoding

Patrick McClure¹, Dustin Moraczewski², Ka Chun Lam¹, Adam Thomas², and Francisco Pereira¹

¹Machine Learning Team, National Institute of Mental Health

²Data Science and Sharing Team, National Institute of Mental Health

Abstract

While deep neural networks (DNNs) are being increasingly used to make predictions from high-dimensional, complex data, they are widely seen as uninterpretable “black boxes”, since it can be difficult to discover what input information is used to make predictions. This ability is particularly important for applications in cognitive neuroscience and neuroinformatics. A saliency map is a common approach for producing interpretable visualizations of the relative importance of input features for a prediction. However, many methods for creating these maps fail due to focusing too much on the input or being extremely sensitive to small input noise. It is also challenging to quantitatively evaluate how well saliency maps correspond to the truly relevant input information. In this paper, we develop two quantitative evaluation procedures for saliency methods, using the fact that the Human Connectome Project (HCP) dataset contains functional magnetic resonance imaging (fMRI) data from multiple tasks per subject to create ground truth saliency maps. We then introduce an adversarial training method that makes DNNs robust to small input noise, and use these evaluations to demonstrate that it greatly improves interpretability.

1 Introduction

Deep neural networks (DNNs) are becoming increasingly used in cognitive and computational neuroscience for a variety of classification and regression tasks from brain imaging data, such as disease diagnosis and prediction of subject traits [1, 2]. In these areas, however, accurate predictions on new subjects are not enough. Knowing what, in input space (e.g. brain structure or brain activation), contains the information that allows the model to make its predictions is often at least as important. In neuroimaging, this information is crucial to developing a deeper understanding of the relationship between brain function and how it manifests in imaging. This will be crucial as translational applications for modulating brain function are developed. The relatively recent availability of very large imaging datasets is starting to allow the development of deep learning models that can outperform classical machine learning techniques in neuroimaging applications [3, 4]. However, their adoption has been slowed, in part, by the perception that such models are inscrutable (i.e. that techniques for producing interpretable visualizations of how input changes affect the output are brittle or challenging to use).

For the specific application of *task decoding* (i.e. predicting which cognitive state a subject is in) from functional magnetic resonance imaging (fMRI) data, the most commonly used models were linear. To interpret their prediction models, the model weights were projected into input space (e.g. regression weights for each voxel) [5, 6]. However, this method does not work for large, non-linear models, such as DNNs. There have been attempts to open up the DNN “black box” by creating *saliency maps*, visualizations of the input space highlighting the features that drive prediction. These saliency

maps are functions of a prediction model *and* a specific input. Two common failure modes for methods that generate saliency maps are that they: (1) generate explanations that are almost entirely a function of the specific input and not sensitive to the learned parameters of the model or (2) generate explanations that dramatically change in the presence of even extremely small input noise [7, 8]. Two proposed methods for dealing with both of these issues are locally smoothing the saliency map [9] and improving the robustness of the DNN to small input noise using adversarial training [10, 11]. However, these methods are often evaluated in situations where getting a quantitative measure of gradient quality is very difficult.

In this paper, we propose two quantitative evaluation criteria for interpretability and use them to compare the performance of different saliency map methods. These criteria take advantage of the fact that, for certain datasets, ground truth saliency maps can be computed. To illustrate the rationale for these evaluation criteria, and compare the quality of the various methods, we carry out these evaluations in a synthetic dataset that mimics brain activation. We, also, apply several saliency-based interpretability methods to linear and DNN models trained to perform fMRI task prediction (i.e. decoding) using the Human Connectome Project (HCP) dataset [12]. Our experimental results indicate that making DNNs robust to small input noise, via adversarial training, can greatly improve the interpretability of saliency maps, without adversely affecting decoding performance.

2 Methods

2.1 Prediction Models

Multinomial Regression In multinomial regression, each class (e.g. decoded task), y_i , has a weight for each input feature (e.g. voxel), resulting in a weight matrix W containing one weight vector \mathbf{w}_i per class. These weights are then multiplied by the input features, \mathbf{x} , to yield a vector $\mathbf{z} = W\mathbf{x}$, containing a logit z_i for each class i . A softmax function, $\sigma(z_i) = \frac{\exp(z_i)}{\sum_j \exp(z_j)}$, is then applied to the resulting vector, computing $\sigma(W\mathbf{x})$. The output of the softmax can be seen as a probability distribution over classes parameterized by W , in other words $p_W(y|\mathbf{x})$. In this paper, we used an L2 regularized multinomial regression model, setting the L2 coefficient using a validation set.

Neural Networks In many cases, a multinomial regression model operating on input features cannot separate all of the classes. Artificial neural networks (NNs) are models that can learn to compute new features that are non-linear functions of the original input features, yielding a new feature space where classes can be separated. A NN consists of functions, often called "layers", applied sequentially. A layer, l , usually takes the form of multiplying the input to the layer, \mathbf{x}_l , by a weight matrix, W_l , and then applying a non-linearity, f_l , resulting in a new set of features $f_l(W_l\mathbf{x}_l)$. For multi-class classification, the final layer usually uses a softmax non-linearity, similar to multinomial regression, producing $p_W(y|\mathbf{x})$.

2.2 Interpretability

2.2.1 Interpreting using Input Gradients

One possible definition of the interpretability of a prediction model is the degree to which it is possible to understand the learned relationship between the input and output variables. For linear regression, this is usually done by looking at the learned weights, as they directly reflect how much changing an input variable would change the output variable (i.e. the gradient of the output with respect to the input). However, linear regression weights are not always straightforward to interpret, as discussed in [13]. In our classification setting, interpretability translates into being able to understand what, in the input space, allows the model to distinguish classes (i.e. how changing the input variables changes the probability of each class).

Formally, this is the gradient with respect to the *input variables*, $\nabla_x p_W(y|x)$. This is different from the gradient with respect to the *learned parameters* of the model, $\nabla_W p_W(y|x)$, which is computed in gradient-based optimization methods to find parameters that make the training data more likely given the model. Note, also, that the gradients for DNNs are dependent on the inputs; this is in contrast to linear regression, which has the same gradient for every input.

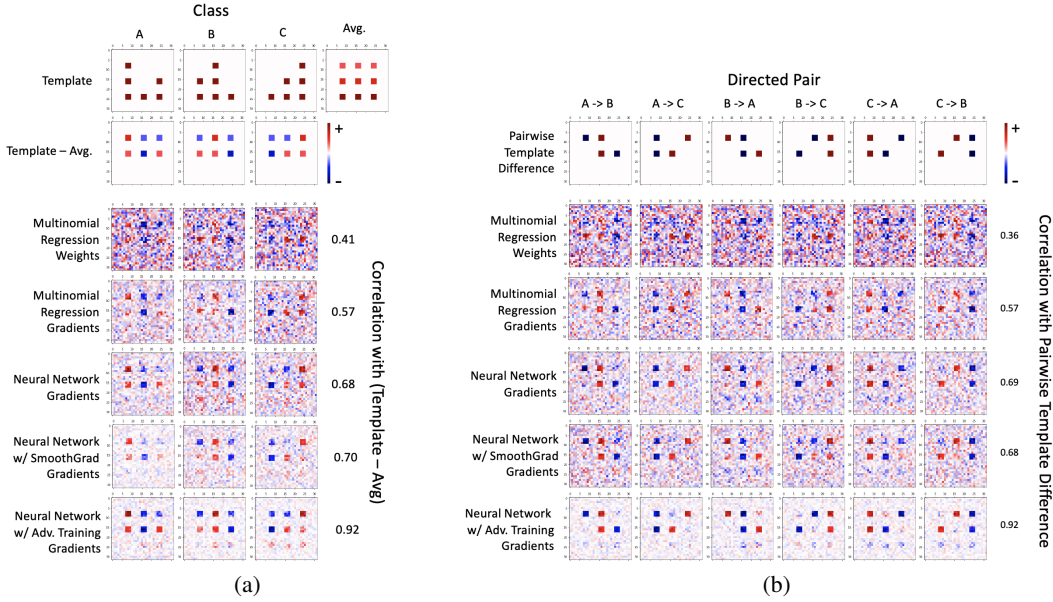


Figure 1: **Visualization of gradient-based saliency maps for synthetic test data predictions, for the two quantitative evaluation criteria we introduce.** **a:** The average saliency maps for the correct class and their correlation with the corresponding "template - average" map. **b:** The average saliency maps for another, incorrect, class and their correlation with the corresponding "pairwise template difference" map.

2.2.2 Quantitative Evaluation of Interpretability

In this article, we propose two quantitative evaluation criteria for the interpretability of gradient-based saliency maps for a classification model. We use them to compare a variety of methods for producing saliency maps, which will be introduced in the rest of this section. The experimental results are presented in Section 3, using both synthetic and real data. Given that it will be easier to describe the evaluation criteria with reference to illustrative examples, we introduce the synthetic dataset here.

The synthetic dataset contains 2D images that are simplified analogues of brain activation maps. The "brain" in these maps can be in one of three classes: A, B, or C. Each class has a characteristic template pattern of activation, made up of 6 activation regions, shown in row 1 of Figure 1a, together with the average of the three templates. The template for one class (e.g. A) has a region that is completely specific to it, and appears in no other class). In addition, it has two other regions that are shared with one of the other classes (e.g. AB and AC). Finally, it has three other regions that are present in all three classes (e.g. ABC).

Our first evaluation criterion aims to answer the question, "What in the input space allows the model to make a correct prediction?" For activation maps, it is whatever activation departs from the average activation across all classes. We quantify this by computing the pixelwise correlation between a saliency map for the correct class of an image and the "template-average" image (i.e. the difference between the correct class template and the average of the three templates) for each test image. We will call this "template-average" image a *class informative activation* map, shown in row 2 of Figure 1a. The values in this map should reflect the relative importance of class-specific versus shared activation that carries some information about the class. This map will be the ground truth for the gradient-based saliency maps produced for each class by the various methods we consider. These are shown in rows 3-7 of Figure 1a, together with their average correlation with the ground truth across test examples.

Our second evaluation criterion aims to answer the question, "What in the input space are the important differences between classes?" The answer to this, given an image of a particular class (e.g. A), are the changes in activation that would be needed to transform it into an image of another class (e.g. B). We will call this the *pairwise class activation difference* map, shown in row 1 of Figure 1b. The saliency map for class B, with a input from class A, should approximate this map. We quantify

this by computing the pixelwise correlation between a saliency map for a class (e.g. B), given an image of another class (e.g. A), and the pairwise class activation difference map (e.g. B-A). This map will be the ground truth for the gradient-based saliency maps produced for each class transformation, by the various methods we consider. These are shown in rows 2-6 of Figure 1b, together with their average correlation with the ground truth across test examples.

2.2.3 Issues with Input Gradients

Unlike the derivative of a logit, the derivative of the probability, $\nabla_x p_W(y|x)$, is dependent on the confidence of the network. This can be an issue if a model is overconfident, since predicted probabilities close to 0 or 1 will make the derivatives be very close to 0. To prevent this, we perform temperature scaling for the evaluated models, as suggested by [14]. In temperature scaling, a temperature parameter, t , is introduced into the softmax function, $\sigma(z)_i = \frac{\exp(z_i/t)}{\sum_j \exp(z_j/t)}$. The temperature parameter can then be set by taking an already trained model, fixing its weights, and finding the t that results in the lowest negative log-likelihood on the validation data. This will result in a model whose predicted probabilities better match the data, since the negative log-likelihood penalizes being confident on incorrect predictions.

An additional complication of using gradients of non-linear models for interpretation stems from the fact the gradients are dependent on the inputs. An advantage of an input-specific gradient is that one can compute which input changes are important for a given example (e.g. what would transform a diseased brain into a healthy one). Conversely, a potential disadvantage is that these input-specific gradients may not directly correspond to important population-level changes.

Another prevalent issue for complex, non-linear models, such as CNNs, is that the gradients, often, are not robust to small input changes. This can cause very similar inputs to have drastically different output probabilities. This reduces the interpretability of gradients and enables easy creation of adversarial examples [8, 11, 15, 16].

2.2.4 SmoothGrad

One popular method for dealing with the lack of robustness in CNN gradients is SmoothGrad [9], which averages out the gradients around an input by estimating $\mathbb{E}_\delta[\nabla_x p_W(y|\mathbf{x} + \delta)]$ where $p(\delta) = \mathcal{N}(\mathbf{0}, I\sigma_\delta^2)$. In practice, Monte-Carlo sampling is used to estimate this expectation by adding random noise, δ , sampled from $p(\delta)$, to an input, calculating the input gradient for each of these noisy inputs, and then averaging over the gradients produced for these different noisy samples. Several papers have reported that this improves the interpretability of CNN gradients [7, 9], although there are no guarantees on this leading to robust gradients. We include SmoothGrad in all experiments, and show the gradients for the synthetic data models in Figure 1.

2.2.5 Adversarial Training

Adversarial training seeks to make a model robust to adversarial examples, by preventing small changes in inputs from dramatically changing the output. This is achieved by creating new training inputs by added adversarial noise. The adversarial noise is determined by calculating the input change that will change the output the most.

Making DNNs robust to small noise has been proposed as means of increasing interpretability [11, 17]. In the original adversarial training papers, the adversarial noise was computed using a gradient step for the input gradient at a real input example, using the fast gradient sign method [15, 16]. Recently, projected gradient descent (PGD) has been proposed to improve the generation of adversarial noise for adversarial training by performing multiple gradient steps when generating adversarial noise [18]. For PGD, the goal is to find the adversarial noise that will either optimally decrease the probability of the correct class of a training input (a.k.a. targeted adversarial noise) or optimally increase the probability of an incorrect class (a.k.a. non-targeted adversarial noise) while staying close to the input example. A common definition of staying close to the input example is restricting the adversarial noise, δ , to have a small L2-norm (i.e. keeping the Euclidean distance between the input example and the adversarial example small). Generating a non-targeted, L2 adversarial example using PGD is achieved by optimizing $\text{argmin}_{\delta_{(\mathbf{x}, y)}} p_W(y|\mathbf{x} + \delta_{(\mathbf{x}, y)})$ s.t. $\|\delta_{(\mathbf{x}, y)}\|_2 \leq \epsilon$.

Adversarial noise can be found by performing this optimization, and then added to the respective input in order to generate an adversarial example. These adversarial examples can then be used to calculate the parameter gradients for one parameter update step. For relatively small models, such as our synthetic data experiment, this can work well. However, this is computationally expensive, and can be prohibitive if using large DNNs. Recently, simultaneously generating adversarial examples by optimizing the adversarial noise and updating the model parameters was proposed [17], which significantly speeds up adversarial training. We developed a version of this method that uses example specific L2 adversarial noise, instead of using universal L_∞ noise. It is described in Algorithm 1.

Algorithm 1 m-step Minibatch Adversarial Training

Require: Set of training minibatches \mathcal{D} , Model parameters W , noise bound ϵ , learning rate τ , hop steps m

- 1: **while** not converged **do**
- 2: **for** minibatch $B \in \mathcal{D}$ **do**
- 3: **for** $(\mathbf{x}, y) \in B$ **do**
- 4: $\delta_{(\mathbf{x}, y)} \leftarrow \mathbf{0}$ ▷ Initialize adversarial noise
- 5: **for** $i = 1, \dots, m$ **do**
- 6: $g_W \leftarrow \mathbb{E}_{(\mathbf{x}, y) \in B} [\nabla_W \log p_W(y|\mathbf{x} + \delta_{(\mathbf{x}, y)})]$ ▷ Get parameter gradients
- 7: $W \leftarrow W + \tau g_W$ ▷ Update parameters
- 8: **for** $(\mathbf{x}, y) \in B$ **do**
- 9: $g_{adv} \leftarrow \nabla_{\mathbf{x}} p_W(y|\mathbf{x} + \delta_{(\mathbf{x}, y)})$ ▷ Get input gradients
- 10: **if** $\|g_{adv}\|_2 > 0$ **then**
- 11: $\nu \sim U(0, \epsilon)$ ▷ Sample adversarial step size
- 12: $\delta_{(\mathbf{x}, y)} \leftarrow \delta_{(\mathbf{x}, y)} - \nu g_{adv} / \|g_{adv}\|_2$ ▷ Update adversarial noise
- 13: **if** $\|\delta_{(\mathbf{x}, y)}\|_2 > \epsilon$ **then**
- 14: $\delta_{(\mathbf{x}, y)} \leftarrow \epsilon \delta_{(\mathbf{x}, y)} / \|\delta_{(\mathbf{x}, y)}\|_2$ ▷ Rescale the adversarial noise

2.3 Related Work on Interpreting Task Decoding Prediction Models

There are many different studies doing task decoding using the Human Connectome Project (HCP) dataset. [6] built several different linear prediction models for a wide variety of tasks across datasets (in addition to HCP, Archi [19], Brainomics [20], and Camcan [21]). [6] projected the weights of multinomial regression models into input space. This is equivalent to looking at the gradient of one the logits with respect to the input. This does not account for the softmax and the weights for all classes, which can lead to reduced interpretability, as illustrated by the comparison of the multinomial regression *weight* and the multinomial regression *gradient* saliency maps in Figure 1.

Several other studies used DNNs, with some type of gradient-based visualization method. [22] trained a 3D convolutional neural network (CNN) to predict the same seven HCP tasks from 4D fMRI data and used guided backprop to visualize input features. However, guided backprop has been shown to not necessarily visualize the input features learned by a CNN [7]. They found that the gradient-based saliency maps had high values in the same location that a general linear model (GLM) activation image in the task had high values. They also found that the saliency maps matched the GLM better than a searchlight [23] analysis. [24] trained LSTM recurrent neural networks (RNNs), with an added input-cell attention mechanism, to decode gambling, relational processing, or working memory from 4D fMRI HCP data. They showed that the added input-cell attention improved the ability to visualize the RNN features of early LSTM layers by computing the gradients of the input with respect to the output, and validated these visualizations using synthetic data. However, the gradient maps used in this study are not robust in general [11]. [25] trained LSTM recurrent neural networks (RNNs) to decode whether a subject was seeing a body, a face, a place, or a tool using 4D fMRI HCP data. They visualized the RNN features using layerwise relevance prop (LRP), which is not robust to small input noise [8]. They found that the resulting gradient maps showed similar patterns to both those found by a GLM and NeuroSynth relevance maps for the different tasks [26].

Across these studies, the saliency methods are mainly evaluated by comparisons to brain activation reference images. They usually ignore that the model is focused on identifying activation that distinguishes each task from others, rather than all of the activation that is present in that task. This paper addresses both this evaluation issue and the above-mentioned problems with the previously

used interpretability methods by: (1) using class-specific information to evaluate interpretability and (2) using the gradients of adversarially robust DNNs in producing saliency maps.

3 Experiments

3.1 Prediction Experiments

3.1.1 Synthetic Data

Data As described in Section 2.2.2, the synthetic dataset contains 2D images that are simplified analogues of brain activation maps in one of three classes: A, B, or C, whose templates are shown on the top row of Figure 1a. Each class activation template contains $32 \times 32 = 1024$ pixels. Each activation region is a 3×3 pixels, square, so $\sim 7\%$ of the "brain" will contain activation in any class. Pixels belonging to an activation region have a value of 1, background pixels have a value of 0. We generated 1000 examples of each class for train, validation, and test sets, respectively. Each example was produced by taking the template for the corresponding class and corrupting it with pixelwise independent Gaussian noise ($\sigma = 0.5$).

Prediction Models and Results We trained both a multinomial linear regression and a NN, which had a 10 unit fully connected layer with ReLU non-linearities and a 7 unit fully connected layer with a softmax non-linearity, to predict which of the three classes (i.e. A, B, or C) generated an image. The NN was trained with and without 3-step PGD adversarial training with $\epsilon = 14$. Each of the models was able to perfectly classify the test data.

3.1.2 fMRI Data

Data For our main evaluation, we used volumetric task fMRI activation maps from the Human Connectome Project 1200 dataset (HCP1200) distribution. Out of 1200 subjects in that distribution, only 965 had volumetric activation maps. We randomly split them into groups of 790 training subjects, 87 validation subjects, and 88 test subjects, respectively. For each subject, HCP1200 contains activation maps for several conditions within each of seven tasks (described in [27]): working memory, gambling, motor, language, social, relational, and emotion. Within our experiments, we treat each task as a class, and we use activation maps of all of the conditions within a particular task as examples of that class, as detailed in Table 1. Input-output pairs, (\mathbf{x}, y) , were created by individually z-scoring these condition beta maps and labelling them with their respective task.

Table 1: The condition to task mapping used to create labels for the HCP data.

HCP Task	Conditions Used
working memory	2-BACK/0-BACK/BODY/FACE/PLACE/TOOL
gambling	PUNISH/REWARD
motor	LF/LH/RF/RH/T
language	MATH/STORY
social	RANDOM/TOM
relational	MATCH/REL/NEG_MATCH/NEG_REL
emotion	FACES/SHAPES/NEG_FACES/NEG_SHAPES

Prediction Models and Results For classifying task from HCP 3D activation maps, we trained an L2-penalized multinomial linear regression model, a 3D CNN, and a 3D CNN with 4-step minibatch adversarial training (Algorithm 1). (See Table 2 for the detailed 3D CNN architecture.) These were all trained using Adam [28]. Hyperparameters, such as the L2 coefficient and adversarial noise bound, were set using the validation data. For adversarial training, the adversarial noise bound, ϵ , was set to 95, which corresponds to a noise of 0.1 (i.e. 10% of a standard deviation) per voxel. The test set accuracies were 74.40%, 93.54%, and 94.03% for the linear model, the CNN, and the CNN with adversarial training, respectively. Both of the CNNs had significantly higher accuracy ($p < 0.001$, corrected) than the linear model, per paired t-tests across test subjects. Also, the use of adversarial training did not significantly change the CNN accuracy ($p > 0.05$, corrected), per a paired t-test across test subjects.

Table 2: The 3D convolutional neural network architecture used for HCP fMRI task decoding.

Layer	Filter	Stride	Padding	Non-linearity	Pooling
1	32x3x3x3	1	1	ReLU	2x2x2 Avg.
2	32x3x3x3	1	1	ReLU	2x2x2 Avg.
3	64x3x3x3	1	1	ReLU	2x2x2 Avg.
4	64x3x3x3	1	1	ReLU	2x2x2 Avg.
5	64x3x3x3	1	1	ReLU	2x2x2 Avg.
6	7x57768256	-	-	Softmax	-

3.2 Evaluation of gradient-based saliency maps

3.2.1 Class Informative Activation

Synthetic data The first criterion introduced in Section 2.2.2 evaluates how well a gradient-based saliency map for a class, generated from an input image with that class, identifies class-informative activation. The ground truth for this, in the synthetic data, is the class informative activation map (the difference between the class template and the average template across all classes). This is shown in row 2 of Figure 1a.

Each gradient-based saliency map method we consider produces, for each example, a map that depends on its class label. The average of these across test examples are shown in rows 3-7 of Figure 1a. The evaluation measure for each test example map is its pixelwise correlation with the class informative activation map, yielding a sample of correlation values. For any two methods, we use a two-sided paired t-test to compare whether their average correlation is different, with Bonferroni correction to account for all of the pairwise comparisons being carried out.

We found that the multinomial regression *gradients* significantly increased the correlation with the class informative activation maps, compared to the multinomial regression *weights* ($p < 0.001$, corrected). This interpretability improvement was expected, because the weights for one class do not take into consideration the softmax and the weights for the other classes. We also found that the NN gradients significantly outperformed the multinomial regression gradients ($p < 0.001$, corrected) and that using SmoothGrad significantly decreased the correlation of the NN gradients with the task informative activation maps ($p < 0.001$, corrected). Adversarial training significantly increased the correlation between the gradient and class informative activation maps compared to the NN gradients ($p < 0.001$, corrected) and the SmoothGrad gradients ($p < 0.001$, corrected).

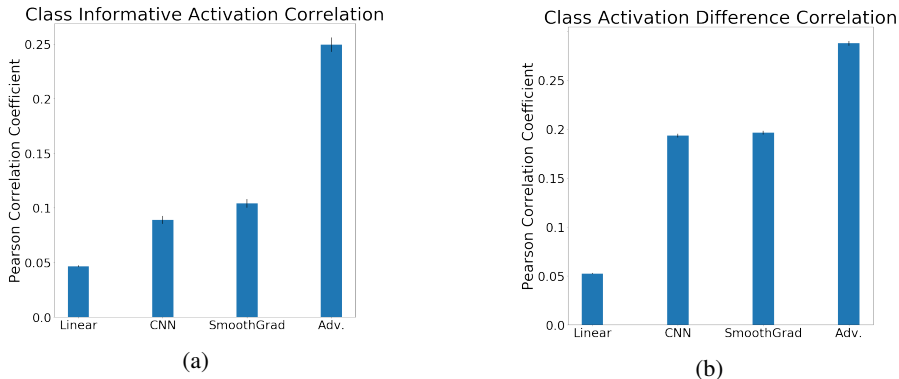


Figure 2: **The average correlations, with standard errors, for gradient-based saliency maps on the HCP test set, for the linear multinomial regression model, convolutional neural network (CNN), CNN with SmoothGrad, and CNN with adversarial training (Adv.). a:** The average correlations versus the task informative activation map, across all test subjects. **b:** The average correlations versus the pairwise class activation difference map, across all tasks and test subjects.

fMRI data We computed a ground truth class informative activation map for each decoding class for each subject, by subtracting a subject’s average example across classes from the subject’s average example of each class. Figure 3a shows the average examples for three classes (row 1), and the

corresponding class informative activation maps (row 2). Note that some classes have highly specific activation (e.g. Language), whereas others share activation with others and hence the activation and class informative activation are visibly different (e.g. Motor). The saliency maps produced with the various methods are shown for one class (Language) in column 1 of Figure 3b.

In order to evaluate each saliency map method, we computed the voxelwise correlation between the map produced for each input example, with the gradient for its correct class, and the class informative activation map. This yields a sample of correlation values for each method; the average correlations for each method are shown in Figure 2a.

Per paired t-tests as described above, the CNN with adversarial noise had a statistically higher correlation ($p < 0.001$, corrected) than all of the other methods, while the linear model had a statistically lower correlation ($p < 0.001$, corrected) than all of the other methods. Additionally, using SmoothGrad significantly ($p < 0.001$, corrected) increased the correlation of the CNN gradients with the task informative activation maps.

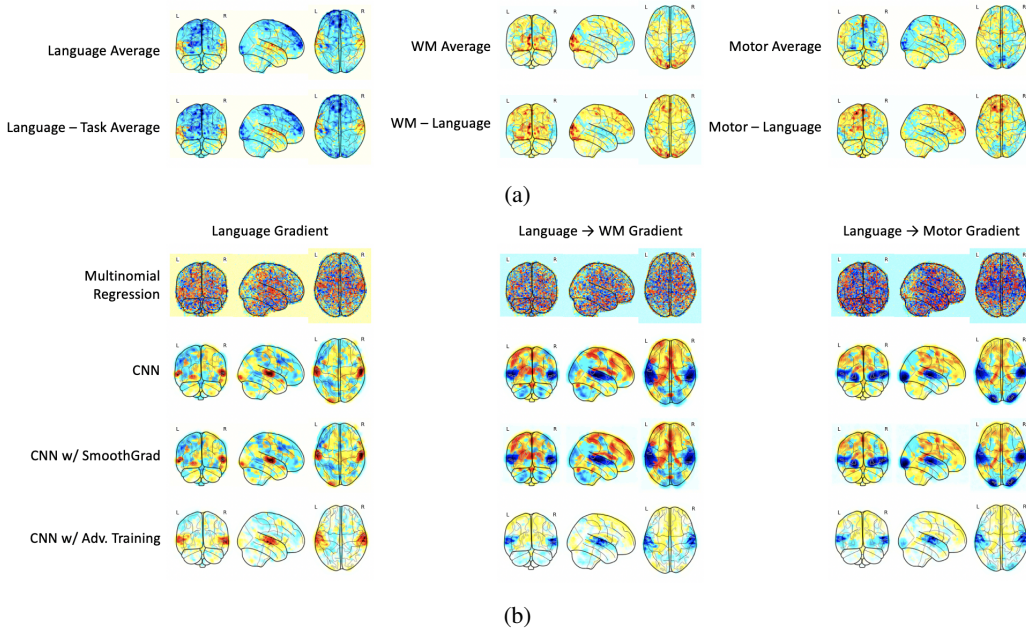


Figure 3: **Visualization of gradient-based saliency maps for a random test subject from the HCP test data.** **a:** In row 1, the coronal, sagittal, and axial views of "glass brains" of the average examples, across conditions, for three classes, Language, Working Memory (WM), and Motor. In row 2, the class informative activation map obtained by subtracting the average example across classes from the average Language example (column 1) and the pairwise class activation difference maps for WM (column 2) and Motor (column 3) with respect to Language. **b:** The average gradient-based saliency maps (rows 1-4) for the Language class, applied to the average example of the Language (column 1), WM (column 2), and Motor (column 3) classes.

3.3 Pairwise Class Activation Differences

Synthetic data The second evaluation criterion introduced in Section 2.2.2 evaluates how well the saliency map for a class B, given an input from class A, identifies the changes in activation that would be needed to transform the input from class A to class B. The ground truth for this, in the synthetic data, is the pairwise class activation difference map, the difference between the template images for classes B and A. This is shown, for every possible transition, in the first row of Figure 1b.

We applied this approach to the saliency maps produced by all of the methods, as shown in rows 2-6 in Figure 1b. For each test example, each method produces a saliency map for each incorrect class, indicating what it would require to transform the example to that class. Each of those saliency maps is then correlated with the corresponding pairwise class activation difference map, yielding an average correlation value across incorrect classes; across test examples, this results in a sample

of correlation values. For any two methods, we used a two-sided paired t-test to determine if their average correlation was different. We used Bonferroni correction to account for all of the pairwise comparisons.

We found that the multinomial regression gradients increased the correlation with the task activation difference maps, compared to the multinomial regression weights ($p < 0.001$, corrected). We also found that the NN gradients significantly outperformed the multinomial regression gradients ($p < 0.001$, corrected) and that using SmoothGrad slightly decreased the correlation of the NN gradients with the task activation difference maps ($p < 0.001$, corrected). Adversarial training lead to a large increase in correlation between the gradient and task activation difference maps compared to both the NN gradients ($p < 0.001$, corrected) and the SmoothGrad gradients ($p < 0.001$, corrected).

fMRI data We computed ground truth class pairwise activation difference maps for each pair of classes for each subject, by subtracting a subject’s average activation map, across conditions, for each class from the average maps of all other classes. We applied this approach to the gradient-based saliency maps for each incorrect class produced for each test example by each of the evaluated methods. In Figure 3b, we show the average gradient-based saliency map produced by each method for the Language class, applied to the average example of the Language (column 1), WM (column 2), and Motor (column 3) classes. Note how these gradient maps remove the most prominent activation in the maps of the correct class (column 1), when transforming to a different class (columns 2 and 3).

For each method, and across all test examples, we correlated the pairwise gradient-based saliency maps with the corresponding pairwise class activation difference maps, yielding an average correlation value across incorrect classes; across test examples, this results in a sample of correlation values. For any two methods, we used a two-sided paired t-test to compare whether their average correlation was different. We used Bonferroni correction to account for all of the pairwise comparisons. The average correlations for the different methods are shown in Figure 2b.) Per two-sided paired t-tests as described earlier, the CNN with adversarial noise had a higher correlation ($p < 0.001$, corrected) than all the other methods, while the linear model had a lower correlation ($p < 0.001$, corrected) than all the other methods. SmoothGrad was significantly better than CNN ($p < 0.001$, corrected).

4 Discussion

In cognitive neuroscience and neuroinformatics applications, interpretability (i.e. understanding how a DNN makes a prediction) is as important as the quality of that prediction. Gradient-based saliency maps have emerged as the main approach to producing an interpretable visualization of which input features are most important in predicting a particular class. They are, however, very sensitive to input noise. Out of various methods proposed to address this problem, we considered SmoothGrad and an adversarial training method that we introduce. In spite of the variety of methods proposed there is, at present, no consensus on the best way to quantitatively evaluate the interpretability of the resulting maps.

In this paper, we introduced two quantitative criteria to evaluate the interpretability of gradient-based saliency map methods. The criteria leverage the fact that we can compute ground truths for such maps for a given input example, for both its correct class and other classes. We first evaluated methods on a synthetic dataset that is a simplified analogue of neuroimaging data, to demonstrate the criteria and verify that they produced the desired quantitative results. We then evaluated them on HCP, a large neuroimaging dataset commonly used for decoding the task being performed by a subject. Prior work attempting to evaluate gradient-based saliency maps in this setting relied on comparing them to external reference images; our approach does not require this. We obtained very consistent results across both synthetic and HCP datasets. First, CNN gradient-based saliency maps have improved interpretability, when compared to standard linear methods. Second, using adversarial training improves the interpretability of CNN gradients, even when compared to SmoothGrad. This indicates that adversarial training is a promising approach, relative to other methods. In terms of future work, the most obvious direction is to address the limitations of using gradients, which are first-order (i.e. linear) and local approximations of the optimization landscape. This would likely further increase the interpretability of complex machine learning models, something that is paramount for their widespread adoption in the scientific community.

Acknowledgements

This work was supported by the National Institute of Mental Health Intramural Research Program (ZIC-MH002968, ZIC-MH002960). This work utilized the computational resources of the NIH HPC Biowulf cluster (<http://hpc.nih.gov>).

References

- [1] T. C. Kietzmann, P. McClure, and N. Kriegeskorte, “Deep neural networks in computational neuroscience,” in *Oxford Research Encyclopedia of Neuroscience*, Oxford University Press, 01 2019.
- [2] M. Khosla, K. Jamison, G. H. Ngo, A. Kuceyeski, and M. R. Sabuncu, “Machine learning in resting-state fmri analysis,” *Magnetic resonance imaging*, 2019.
- [3] A. Abrol, Z. Fu, M. Salman, R. Silva, Y. Du, S. Plis, and V. Calhoun, “Hype versus hope: Deep learning encodes more predictive and robust brain imaging representations than standard machine learning,” *bioRxiv*, 2020.
- [4] S.-M. Khaligh-Razavi and N. Kriegeskorte, “Deep supervised, but not unsupervised, models may explain it cortical representation,” *PLoS computational biology*, vol. 10, no. 11, 2014.
- [5] F. Pereira, T. Mitchell, and M. Botvinick, “Machine learning classifiers and fMRI: A tutorial overview,” *Neuroimage*, vol. 45, no. 1, pp. S199–S209, 2009.
- [6] A. Mensch, J. Mairal, D. Bzdok, B. Thirion, and G. Varoquaux, “Learning neural representations of human cognition across many fMRI studies,” in *Advances in Neural Information Processing Systems*, pp. 5883–5893, 2017.
- [7] J. Adebayo, J. Gilmer, M. Muelly, I. Goodfellow, M. Hardt, and B. Kim, “Sanity checks for saliency maps,” in *Advances in Neural Information Processing Systems*, pp. 9505–9515, 2018.
- [8] P.-J. Kindermans, S. Hooker, J. Adebayo, M. Alber, K. T. Schütt, S. Dähne, D. Erhan, and B. Kim, “The (un) reliability of saliency methods,” in *Explainable AI: Interpreting, Explaining and Visualizing Deep Learning*, pp. 267–280, Springer, 2019.
- [9] D. Smilkov, N. Thorat, B. Kim, F. Viégas, and M. Wattenberg, “Smoothgrad: Removing noise by adding noise,” *arXiv preprint arXiv:1706.03825*, 2017.
- [10] B. Kim, J. Seo, and T. Jeon, “Bridging adversarial robustness and gradient interpretability,” *arXiv preprint arXiv:1903.11626*, 2019.
- [11] D. Tsipras, S. Santurkar, L. Engstrom, A. Turner, and A. Madry, “Robustness may be at odds with accuracy,” in *International Conference on Learning Representations*, 2018.
- [12] D. C. Van Essen, S. M. Smith, D. M. Barch, T. E. Behrens, E. Yacoub, K. Ugurbil, W.-M. H. Consortium, *et al.*, “The WU-Minn human connectome project: An overview,” *Neuroimage*, vol. 80, pp. 62–79, 2013.
- [13] N. Kriegeskorte and P. K. Douglas, “Interpreting encoding and decoding models,” *Current Opinion in Neurobiology*, vol. 55, pp. 167–179, 2019.
- [14] C. Guo, G. Pleiss, Y. Sun, and K. Q. Weinberger, “On calibration of modern neural networks,” in *Proceedings of the 34th International Conference on Machine Learning*, vol. 7, pp. 1321–1330, JMLR. org, 2017.
- [15] C. Szegedy, W. Zaremba, I. Sutskever, J. Bruna, D. Erhan, I. Goodfellow, and R. Fergus, “Intriguing properties of neural networks,” *arXiv preprint arXiv:1312.6199*, 2013.
- [16] I. J. Goodfellow, J. Shlens, and C. Szegedy, “Explaining and harnessing adversarial examples,” *arXiv preprint arXiv:1412.6572*, 2014.
- [17] A. Shafahi, M. Najibi, M. A. Ghiasi, Z. Xu, J. Dickerson, C. Studer, L. S. Davis, G. Taylor, and T. Goldstein, “Adversarial training for free!,” in *Advances in Neural Information Processing Systems*, pp. 3353–3364, 2019.
- [18] A. Madry, A. Makelov, L. Schmidt, D. Tsipras, and A. Vladu, “Towards deep learning models resistant to adversarial attacks,” *arXiv preprint arXiv:1706.06083*, 2017.

- [19] P. Pinel, B. Thirion, S. Meriaux, A. Jobert, J. Serres, D. Le Bihan, J.-B. Poline, and S. Dehaene, “Fast reproducible identification and large-scale databasing of individual functional cognitive networks,” *BMC Neuroscience*, vol. 8, no. 1, p. 91, 2007.
- [20] D. P. Orfanos, V. Michel, Y. Schwartz, P. Pinel, A. Moreno, D. Le Bihan, and V. Frouin, “The brainomics/localizer database,” *Neuroimage*, vol. 144, pp. 309–314, 2017.
- [21] M. A. Shafto, L. K. Tyler, M. Dixon, J. R. Taylor, J. B. Rowe, R. Cusack, A. J. Calder, W. D. Marslen-Wilson, J. Duncan, T. Dalgleish, *et al.*, “The cambridge centre for ageing and neuroscience (Cam-CAN) study protocol: a cross-sectional, lifespan, multidisciplinary examination of healthy cognitive ageing,” *BMC Neurology*, vol. 14, no. 1, p. 204, 2014.
- [22] X. Wang, X. Liang, Z. Jiang, B. A. Nguchu, Y. Zhou, Y. Wang, H. Wang, Y. Li, Y. Zhu, F. Wu, *et al.*, “Decoding and mapping task states of the human brain via deep learning,” *arXiv preprint arXiv:1801.09858*, 2018.
- [23] N. Kriegeskorte, R. Goebel, and P. Bandettini, “Information-based functional brain mapping,” *Proceedings of the National Academy of Sciences*, vol. 103, no. 10, pp. 3863–3868, 2006.
- [24] A. A. Ismail, M. Gunady, L. Pessoa, H. C. Bravo, and S. Feizi, “Input-cell attention reduces vanishing saliency of recurrent neural networks,” in *Advances in Neural Information Processing Systems*, pp. 10813–10823, 2019.
- [25] A. W. Thomas, H. R. Heekeren, K.-R. Müller, and W. Samek, “Analyzing neuroimaging data through recurrent deep learning models,” *Frontiers in Neuroscience*, vol. 13, p. 1321, 2019.
- [26] T. Yarkoni, R. Poldrack, T. Nichols, D. Essen, and T. Van Wager, “NeuroSynth: A new platform for large-scale automated synthesis of human functional neuroimaging data,” *Front. Neuroinform.* 5, 2011.
- [27] D. M. Barch, G. C. Burgess, M. P. Harms, S. E. Petersen, B. L. Schlaggar, M. Corbetta, M. F. Glasser, S. Curtiss, S. Dixit, C. Feldt, *et al.*, “Function in the human connectome: Task-fMRI and individual differences in behavior,” *Neuroimage*, vol. 80, pp. 169–189, 2013.
- [28] D. P. Kingma and J. Ba, “Adam: A method for stochastic optimization,” *arXiv preprint arXiv:1412.6980*, 2014.